Experimental investigation of the macroscopic flow of He II due to an oscillating grid in the zero temperature limit

H. A. Nichol,[1] L. Skrbek,[2] P. C. Hendry,[1] and P. V. E. McClintock[1]
[1]*Department of Physics, Lancaster University, Lancaster LA1 4YB, United Kingdom*
[2]*Joint Low Temperature Laboratory, Institute of Physics ASCR and Charles University, V Holešovičkách 2, 180 00 Prague, Czech Republic*
(Received 12 May 2004; published 17 November 2004)

A systematic experimental investigation of the macroscopic flow properties of extremely pure He II in the zero temperature limit is reported, covering the pressure range $0.3 < P < 24.8$ bar. The flow is generated by electrostatically driven oscillations of a thin, tightly stretched, circular, square-mesh nickel grid. With growing amplitude of oscillation, the flow changes character at a first critical threshold from pure inviscid superflow past a submerged body of hydrodynamically enhanced mass, to a flow regime that is believed to involve a boundary layer composed of quantized vortex loops. Here the oscillatory motion of the grid acquires strongly nonlinear features. These include double-valued (reentrant) resonance curves and a decrease in the resonant frequency with increasing drive amplitude, but without any appreciable increase in damping. On further increase of the drive level, a second critical threshold is attained: here, the resonant frequency reaches a stable value, the response amplitude almost stops growing, but the linewidth increases. Finally, the flow acquires the character of fully developed classical turbulence, characterized by a square-root dependence of flow velocity on the driving force. Additional flow features attributable to the presence of remanent vorticity are observed and discussed.

DOI: 10.1103/PhysRevE.70.056307 PACS number(s): 47.27.Cn, 47.37.+q, 67.40.Vs, 47.15.Cb

I. INTRODUCTION

Ever since the discovery of superfluidity more than a half century ago, the exotic flow properties of superfluid He II have been subjected to intense investigation, leading to the accumulation of a vast experimental database and a great deal of theoretical knowledge (see, e.g., Refs. [1–3] and references therein). Nevertheless the problems of He II flow, together with complex flow properties of other quantum fluids, are still far from being settled.

Some features of He II flow at finite temperature are firmly established. In the limit of low velocity, He II flow is very well described within the framework of the two-fluid model originally proposed by Landau [4,5]. His description assumes that the viscous normal fluid and inviscid superfluid move in such a way that their velocity fields are independent. One great achievement of this model was the prediction of *second sound*, which involves a counteroscillation of these two components. Landau's predicted critical velocity for roton creation is seldom attained [6], however. Rather, in macroscopic flow beyond a certain threshold, quantized vortices appear in the liquid. The magnitude of this threshold depends on the precise geometry of the flow in question, and the generating mechanism can either be intrinsic [7,8], i.e., where the vortices are created *ab initio* in the superfluid, or extrinsic, i.e., where growth occurs from preexisting (remanent) vortices already present in the superfluid. Macroscopic flow always seems [2] to be characterized by extrinsic vortex creation. Quantized vortices couple together the originally independent normal and superfluid velocity fields in a complicated way, creating a *mutual friction* between them. Note that here, and in what follows, we use the term *macroscopic* of flows that are large on the scale of atoms, and which are not appreciably affected by adding/removing one or a few quantized vortex loops or by a slight change in their topology. This is in contradistinction to the *microscopic* flows that result from one or only a few individual vortex loops.

In the temperature range where He II contains an appreciable proportion of normal fluid, say above about 1.2 K, numerous investigators have observed that, on exceeding a suitably defined Reynolds number, He II flow acquires an increasingly classical character. For example: (i) the He II surface within a bucket rotating with sufficient angular velocity forms a nearly parabolic classical meniscus [9]; (ii) flow of He II past a sphere displays both laminar and turbulent drag [10–12]; (iii) flow of He II past a sphere can also exhibit a drag crisis [13]; (iv) the energy spectrum of turbulent He II involves an inertial range [14] with a classical Kolmogorov roll-off exponent of $-5/3$; and (v) the decay of quantum turbulence in He II, whether generated by towing a grid through a stationary sample [15–19], or by normal fluid/superfluid counterflow, displays classical features [20].

Although such behavior is typically observed over a temperature range within which the proportion of normal fluid to superfluid changes widely, it is impossible to exclude the possibility that this classical-like behavior is associated with the presence of the viscous normal fluid. There is thus a clear call to study the macroscopic properties of He II flow in the zero temperature limit, where normal fluid is (almost) absent and the flow of the superfluid can therefore be investigated in its pure form. The task seems particularly topical in view of experiments with a tiny sphere [10,11] and a very thin vibrating wire [21] displaying intriguing features attributable to single vortices. The purpose of the present work is to investigate how He II changes its properties from pure superfluid (inviscid) potential flow to turbulence as the flow

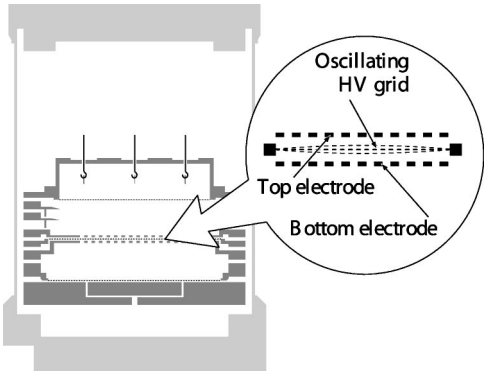

FIG. 1. Schematic drawing showing the geometry of the experimental cell.

velocity increases. As we shall see, there is a clearly defined intermediate stage between these two extremes where there seems to be a boundary layer of quantized vortices that do not produce viscous effects, but can exert a dynamical influence when the flow velocity changes. We infer that this evolution is probably an inherent, temperature-independent, property of He II in large scale flow.

Our tool is of macroscopically large dimensions—an 8 cm diameter oscillating grid, driven near its resonant frequency in isotopically pure He II at low temperature. A preliminary report of this work has already been published [22]. The present paper provides a more detailed account of our experiments and is organized as follows: Sec. II describes our experimental setup; in the central Sec. III we present our experimental results; we discuss them in Sec. IV; and we summarize and draw conclusions in Sec. V.

II. EXPERIMENTAL ARRANGEMENTS

The experiments were performed in an Oxford Instruments Kelvinox 100 ^{3}He/^{4}He dilution refrigerator with a cooling power exceeding 110 μW at 100 mK and a base temperature of <9.2 mK. The sample of istopically pure ^{4}He (^{3}He content below 10^{-13}) was prepared using a thermal counterflow technique [23]. No part of the gas-handling system—neither the storage bottle, high pressure tubing, valves, cold traps, nor bomb—had ever been exposed to natural helium, thus avoiding any possibility of contamination [24]. Pressures up to the solidification pressure of 25 bar could be maintained and measured by a high precision Texas Instruments pressure gauge.

The experimental cell [6] is shown schematically in Fig. 1. It has a stainless steel body, with a stainless steel and copper cap, and is of about 1.5 l capacity. Inside the cell there are two metal film heaters and six resistance thermometers, the principal one being a Lake Shore Cryogenics calibrated germanium diode.

The vibrating grid components consist of two plates sandwiching the high voltage grid with $d=1$ mm spacings between the grid and each plate. The plates are 1 mm thick disks of gold plated copper, with 170 $\sim$2 mm holes drilled in a hexagonal pattern. The grid is in the form of a circular membrane, $2R=8$ cm in diameter, tightly stretched on a circular mild steel carrier. The membrane is cut from Micromesh 200 lines-per-inch electroformed nickel grid material of density $\varrho_G=8.902$ g cm^{-3}. The grid is of a mesh size 127 μm and of 70% effective transparency. It is shown in electron micrographs and schematically in Fig. 2. Note that, on a scale of 1–2 μm, the grid is considerably rougher on one side than on the other, as can be seen in the lower part of the figure. A static potential, typically of $V_0=500$ volts, is applied to the grid and an oscillatory driving potential $V_1=V_{10}\cos\omega t$ ($V_{10}\ll V_0$) applied to the upper electrode provides a net driving force on the grid of the form

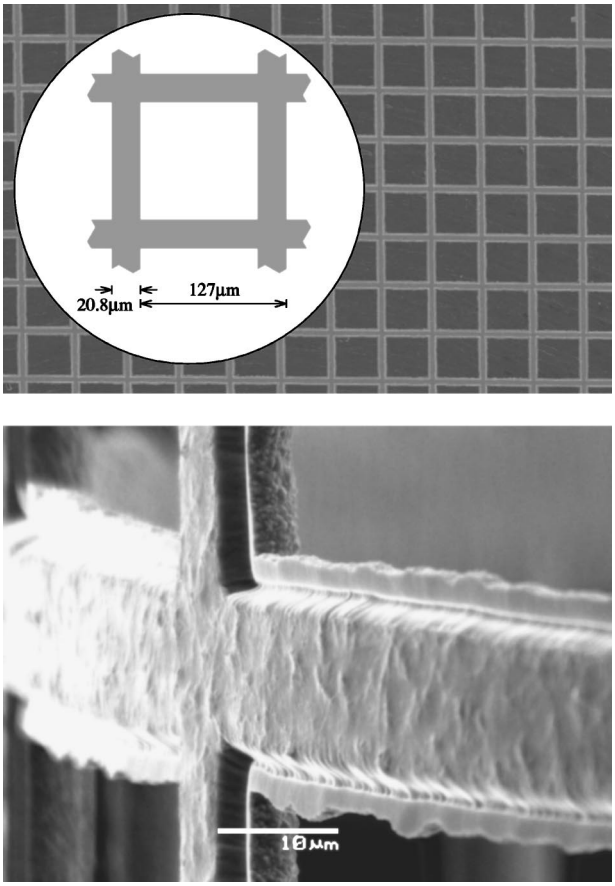

FIG. 2. Electron micrographs of the grid (sample cut from the same sheet), together with a schematic drawing (upper part of figure). The grid wires are not perfectly rectangular in cross section (lower part), and they are rougher on on their back surfaces than on their fronts (see right hand edge of vertical wire).

$$f_d=\varepsilon_0\varepsilon_r\pi R^2V_0V_1/d^2, \tag{1}$$

where ε_0 and ε_r denote, respectively, the permitivity of free space and the relative permitivity of liquid ^{4}He. The grid thus represents an oscillating membrane under uniform tension [27]. Approximating its motion as one dimensional, and assuming that the oscillation amplitude is uniform across its area [22,27], it is easy to show that oscillations of amplitude ΔD induce an oscillatory voltage of amplitude

$$V_2=V_0\Delta D/d \tag{2}$$

on the lower electrode. The capacitance $C_c\cong 700$ pF of the connecting cable and the input capacitances of the measuring

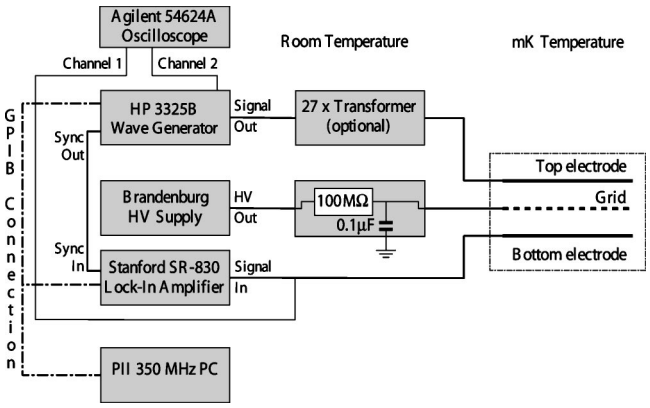

FIG. 3. Schematic block diagram of the experiment, showing the main components used for the measurements.

devices reduce the induced voltage V_2 by a factor of $(1+C_c/C)^{-1}$, where $C \cong 47$ pF is the capacitance between the grid and the lower copper electrode. Subject to this reduction factor [28], the response amplitude $|V_2|$ provides a direct measure of the amplitude and peak velocity $|v_g|=|\omega \Delta D|$ of the oscillating grid [29].

A Hewlett Packard HP3325B synthesizer/function generator is used to provide the drive voltage for the top electrode. Its output spans the range from 0.001 V_{pp} to 10 V_{pp}; use of a 27× step up transformer extends the range to 270 V_{pp}, thus encompassing more than five orders of magnitude in total, and allowing the flow to be probed over a correspondingly wide dynamical range. A Brandenburg high voltage supply provides the grid bias via an *RC* filter to attenuate 50 Hz and other noise. The signal picked up on the bottom electrode can be monitored either with a Stanford Research SR-830 lock-in amplifier, or with an Agilent 54624A oscilloscope to allow direct visualization of transient processes arising at the higher drives. These devices are linked (see Fig. 3) via the GPIB interface to a personal computer (PC) using the LABVIEW 5.0 software package.

III. EXPERIMENTAL RESULTS ON FLOW DUE TO THE OSCILLATING GRID

In this section, we describe our experimental observations on the behavior of the grid oscillating in vacuum and compare them with those in He II at various pressures. In each case, the grid was driven by the same spatially uniform harmonic driving potential in the vicinity of the resonant frequency of its fundamental axisymmetric (0,1) mode [30]. As we will see, the response amplitude as a function of frequency can be highly non-Lorentzian. When we use terms like at *resonance* or *resonant frequency* in such cases, we are referring to the frequency of maximum response. The main results are presented in Figs. 4 and 5, which we discuss in detail below.

A. Resonant response of the grid in vacuum

The vacuum experiments were performed at low temperature using exactly the same setup as for He II. The cell was alternately evacuated and flushed with dry nitrogen gas at room temperature to ensure that it was completely free of residual ^{4}He, which would have formed a creeping film and altered the mass and resonant frequency of the grid. For low and moderately high drive levels the resonant response is of a Lorentzian form with a quality factor $Q \sim 10^4$, as seen in Fig. 4(a). The resonant frequency depends only very weakly on the driving amplitude: a plot of frequency against the square root of the drive yields a straight line, giving the resonant frequency of the (0,1) oscillatory mode in vacuum in the limit of zero amplitude as $f_0=(1117.20\pm0.05)$ Hz. For high drive levels the resonant response versus drive becomes visibly sublinear, (see Fig. 6), presumably due to approaching the elastic limit of the grid material [32]. This phenomenon occurred gradually, and at higher response amplitude than that for the onset of nonlinearity when driving the grid in He II (see below).

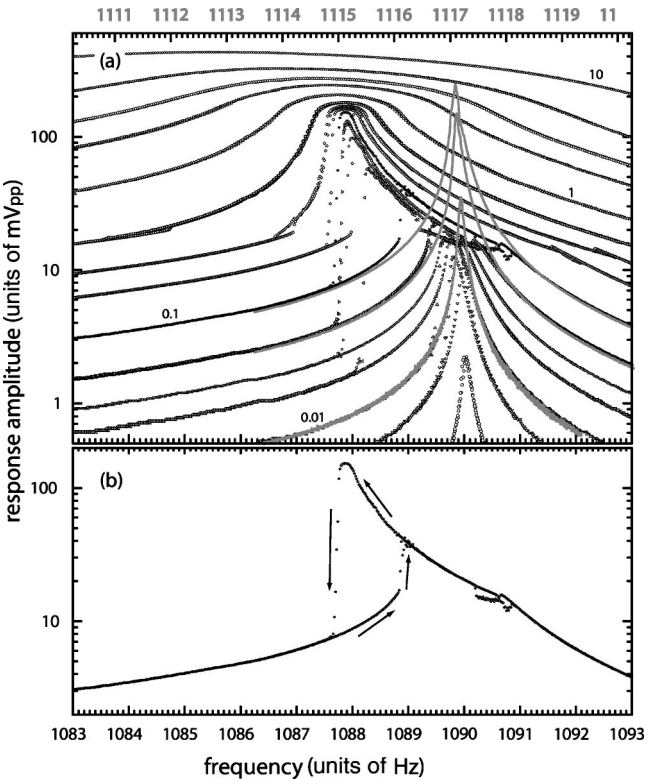

FIG. 4. (a) Resonance curves measured with the lock-in amplifier at 5.05 bar for drive levels (in V_{pp}) of 0.001, 0.005, 0.01, 0.02, 0.03, 0.05, 0.1, 0.2, 0.3, 0.5, 1, 2, 3, 5, and 10. Each drive level is represented by two separate curves recorded for frequency sweeps in opposite directions. There is an intermediate range of driving levels where hysteresis loops with two stable branches arise but, otherwise, the two sweeps produce identical results. The superimposed (almost) Lorentzian resonances (smooth, gray-scale) represent the responses to 0.01, 0.05 and 0.1 V_{pp} drives in vacuum (upper frequency axis). (b) For clarity, a separate plot of the data for the 0.2 V_{pp} drive is shown as an example of results recorded at intermediate drive amplitude. The arrows indicate direction around the hysteresis loop.

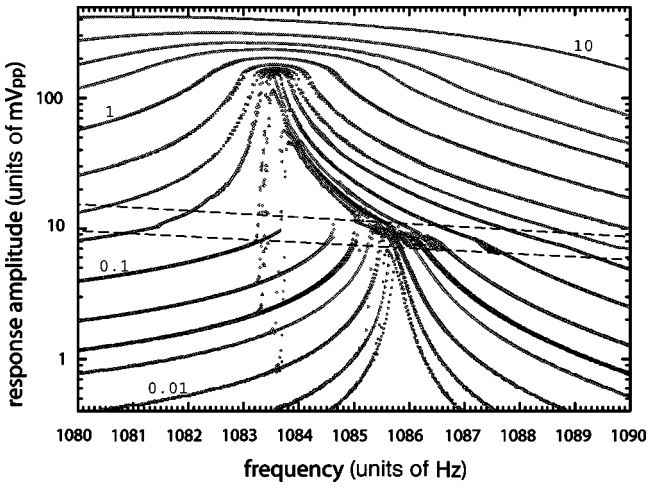

FIG. 5. Resonance curves measured with the lock-in amplifier at 24.79 bar for drive levels (in V_{pp}) of 0.003, 0.005, 0.01, 0.02, 0.03, 0.05, 0.1, 0.2, 0.3, 0.5, 1.0, 2.0, 3.0, 5.0, and 10.0. Each drive level is represented by two separate curves recorded for frequency sweeps in opposite directions. There is an intermediate range of driving levels where hysteresis loops with two stable branches arise but, otherwise, the two sweeps produce identical results. The dashed lines—guides to the eye—indicate the position of the first critical threshold. Note that its vertical position is shifted down slightly compared with Fig. 4. Otherwise, the behavior is very similar to that at 5.05 bar.

B. "Regular" resonant response of the grid in He II

We refer to the resonant response of the grid as becoming *regular* after violently shaking it by means of the highest

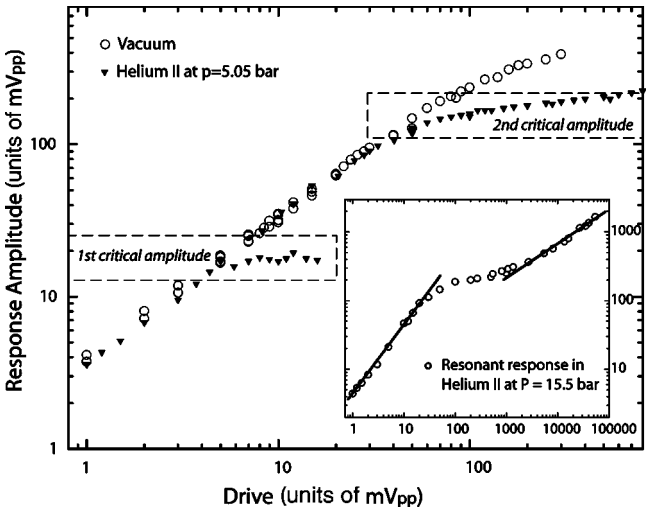

FIG. 6. Response amplitude of the grid versus the drive level at resonance measured in vacuum (open symbols) and in He II at $p=5.05$ bar (main figure). The positions of the first and the second thresholds are indicated in order to emphasize that above the first threshold the damping remains unchanged, provided the measurements are recorded in sequence from high drive toward low drive. The inset shows the drive dependence of the response amplitude of the grid at $p=15.5$ bar, indicating regions of laminar and turbulent flow regimes. The full lines indicate the linear and square-root responses.

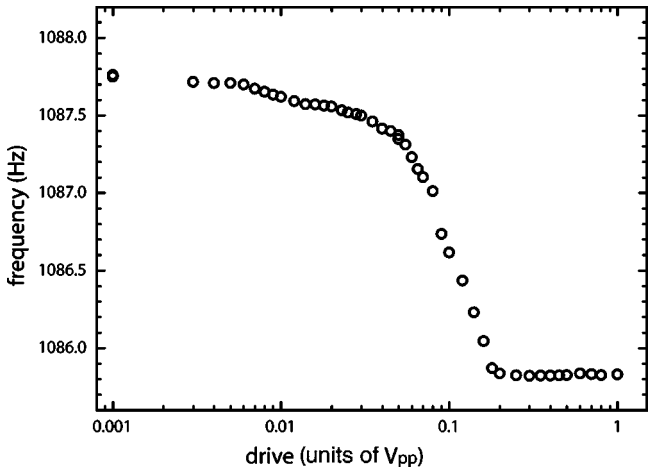

FIG. 7. The drive dependence of the resonance frequency measured at 10 bar using the lock-in amplifier.

available drive ≈ 10 V_{pp} (without use of the transformer). This procedure was applied every time the pressure in the cell was altered, especially when the pressure was increased; in its absence, the resonant frequency tended to be irreproducible. The regularization is believed (see below) to correspond to remanent vortex lines being shaken off the grid, or rearranged on it while still remaining attached. Following this "cleaning" procedure, the behavior of the grid was found to be stable on a time scale of days, in that its resonant frequency f_1 in the limit of low drive was reproducible within typically ± 0.1 Hz.

For the several pressures at which data were recorded within the range $0.30 \leqslant p \leqslant 24.79$ bar, the response of the nearly-resonantly-driven grid was essentially unchanged. The same interesting characteristic features were observed, with only relatively weak quantitative dependences on pressure. We therefore take as typical the data sets obtained at $p=5.05$ bar (Fig. 4) and $p=24.79$ bar (Fig. 5), and use these for a qualitative discussion of the results.

For low drives, the resonant response has the usual Lorentzian line shape, with a quality Q factor comparable to that measured in vacuum: see the superimposed vacuum resonances in Fig. 4. The resonant frequency shifts down slightly with increasing drive amplitude, roughly in the manner expected of a lightly damped linear oscillator (see Fig. 7). As the drive increases further, the grid amplitude reaches a first critical threshold (typically 10–20 mV_{pp}, corresponding to a mean grid velocity of $0.08 < v_g^{(1)} < 0.24$ cm/s) [31]. Subsequently, the oscillation amplitude at resonance still continues to rise in proportion to the drive (see Figs. 4–6), the resonant frequency rather suddenly starts decreasing much faster (see Fig. 7), and the resonance curves acquire highly nonlinear features.

To illustrate more clearly the hysteretic behavior observed in the range of intermediate driving amplitude, the resonance curve for a drive of 0.2 V_{pp} is replotted on its own as an example in Fig. 4(b). As the driving frequency is gradually reduced from 1093 Hz (in practice, incrementally, in steps of typically 0.001 Hz), the system initially continues to display a nearly Lorentzian stationary response. At the first thresh-

TABLE I. Observed values characterizing He II flow due to the oscillating grid at various pressures: f_1 and f_2 are, respectively, the resonant frequencies in the limit of low drive (~ 0.003 V_{pp}) and for the drive level needed to bring the system to the second threshold; V_1 stands for the peak amplitude response of the first and V_2 of the second threshold (for explanation, see text).

p (bar)	f_1 (Hz)	f_2 (Hz)	V_1 (mV_{pp})	V_2 (mV_{pp})
0.30	1091.15	1088.88	19.9	189.1
2.20	1090.45	1088.39	19.3	189.1
3.50	1090.41	1088.10	19.5	188.0
5.05	1089.95	1087.87	17.1	188.2
5.50	1089.75	1087.75	19.9	190.7
10.0	1087.82	1085.78	19.5	190.6
10.09	1087.75	1085.79	17.5	189.0
12.05	1087.50	1085.55	16.3	192.2
14.00	1087.40	1085.29	16.0	191.2
15.50	1086.80	1085.06	24.1	188.5
15.55	1086.90	1085.01	10.5	190.8
18.00	1086.85	1084.60	8.90	192.5
19.95	1086.50	1084.28	10.1	188.4
24.79	1085.75	1083.57	9.70	193.2

old, however, there is a distinct change in the local gradient of the response-frequency characteristic: the response continues to rise with decreasing frequency, but more slowly than before. This continues until at about 1087.7 Hz, just after passing through a maximum, the response amplitude suddenly collapses down onto a lower stable branch. It then decreases smoothly with further reduction in frequency. On increasing the drive frequency again the system stays on the lower branch until, at about 1088.8 Hz where the first threshold is attained, a transition to the stable upper branch occurs. These hysteretic loops are stable. One can circle them many times, providing that the frequency is changed very slowly or in small steps. They have mostly been measured at temperatures around 50 mK, but are not appreciably affected by an increase of temperature up to our maximum of 130 mK. It appears, therefore, that they represent phenomena occurring in the zero temperature limit of He II flow.

As a guide to the eye, Fig. 5 contains a pair of dashed lines marking approximately the first critical threshold. This threshold is clearly visible on all resonance curves (of which we have measured about three times more than are shown at this pressure, though for clarity not all are displayed) and slightly decreases with increasing frequency. The same feature occurs at all pressures. As a quantitative measure of this first threshold we have chosen the response amplitude V_1 in mV_{pp} at which the jump from the lower to the upper branch occurs while slowly sweeping the frequency up under 0.1 V_{pp} drive. Table I contains these observed values for all investigated pressures.

In Fig. 4 the resonance curves measured in vacuum are superimposed on the data obtained for the same drive levels in He II at $p=5.05$ bar. The low response parts of these two sets of resonance curves are seen to coincide closely, provided that the frequency scale (upper axis) is shifted down by about 30 Hz; the same procedure can be carried out for data at any pressure. Above the first threshold, however, the response in He II is drastically different from that in vacuum.

The downshift in frequency with increasing drive reaches a maximum value of ≈ 2 Hz (see Fig. 7) at all pressures, ceasing at a second critical threshold amplitude $\simeq 190$ mV_{pp}. Unlike the first critical threshold, the second threshold amplitude is almost pressure independent (see Table I).

With further increase in drive, the oscillation amplitude at resonance initially remains almost constant, while the widths of the resonance curves increase rapidly (see Figs. 4 and 5). Only for drive levels exceeding by about an order of magnitude that needed to reach the second threshold does the amplitude at resonance grow again; this time approximately in proportion to the square root of the drive, as shown in the inset of Fig. 6. In this high drive regime the linewidth increases rapidly while the resonant frequency decreases gradually, qualitatively in the manner expected for growing damping. Experiments in this regime involve a rather tedious procedure. Driving the grid very hard results in considerable heating of the cell. The measurements were done in such a way that the high level drive was applied only briefly, for the ~ 5 s needed to obtain a stable signal and read out the data point digitally from the oscilloscope; it then took about an hour for the temperature of the cell to decrease back to its previous level. The temperatures at which the upper part of the drive dependence curve in Fig. 6 was measured are thus poorly defined, and might have been significantly higher than the nominal ~ 50 mK where most of the measurements were made.

There are thus two well-defined resonant frequencies that have been observed at each investigated pressure: the resonant frequency f_1 in the zero drive limit; and the resonant frequency f_2 at the second threshold, where the frequency downshift with amplitude ceases. Their values are given in Table I. Figure 8 plots f_1 as a function of He II density (circles). The line represents a least-squares linear fit to these data, also including the zero density resonant frequency f_0 measured in vacuum under the same conditions. It is evident that, in the low drive limit, the resonant frequency decreases linearly with density. The triangles show that the resonance also varies with density in a similar manner near the second critical threshold. Within our experimental accuracy, the observed frequency shift $\Delta f = f_1 - f_2$ does not depend on pressure, as indicated in Fig. 9.

The response amplitude of the grid *at resonance* is plotted as a function of drive amplitude in Fig. 6. While increasing the drive amplitude, the system seems to encounter a nucleation problem when passing the first threshold: on some occasions the response stopped growing with increasing drive level (as indicated by several points at the level of the first threshold), and jumped onto the usual response/drive curve only later. With decreasing drive this feature was absent, and the response remained always proportional to the drive level. However, when measuring the drive dependence of the response amplitude of the grid at a *fixed frequency* near the resonance, hysteresis occurs in the part of the parameter space where the resonance curves are multivalued. Further away from the resonance, the drive dependence is nonlinear

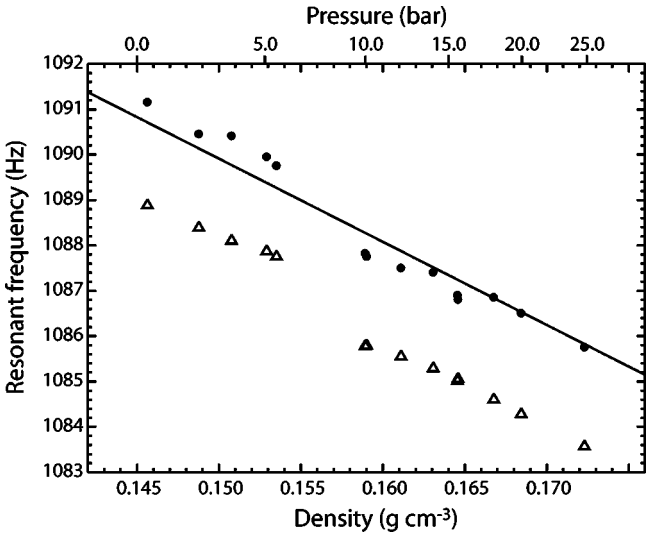

FIG. 8. Resonant frequency as a function of He II density at low drive levels (circles) and for the second critical threshold (triangles). The straight line extrapolates through the zero density (vacuum) resonant frequency of $f_0=1117.2$ Hz. The corresponding pressures are marked on the upper abscissa. This shift of resonant frequency with density is due to the change in the classical hydrodynamic effective mass (see text).

but single valued, as illustrated in Fig. 3 of our preliminary report [22].

C. Amplitude modulation phenomena

Our preliminary report contains a central figure (Fig. 2) showing the resonance curves that correspond to various drive levels measured at 10 bar using the memory oscilloscope. Direct visualization of the grid response in this way has the advantage of allowing us to identify areas in the parameter space where an unexpected amplitude modulation of the response occurred. As displayed on the oscilloscope (Fig. 10) the phenomenon looks similar to beats between oscillations of comparable amplitude but slightly different frequency, so we will refer to it as stable *beating*. Based on observations at several pressures, we can summarize their main features.

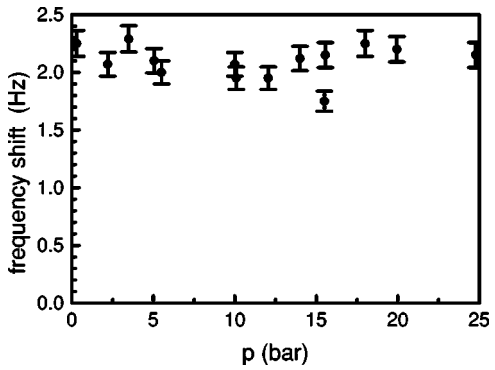

FIG. 9. Downshift in resonant frequency, f_1-f_2, between the first and second critical thresholds plotted as a function of pressure.

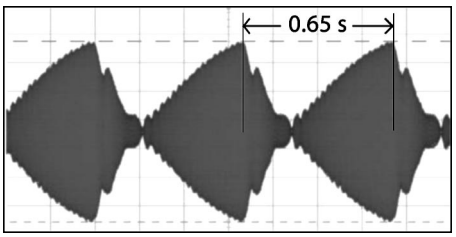

FIG. 10. The response amplitude of the grid driven in He II near its resonant frequency in a regime of steady beating, as obtained on the screen of the memory oscilloscope. Note that on this time scale it is the envelope of the oscillation amplitude that is seen, not the individual oscillations.

(i) The modulation frequency is typically ~1 Hz.

(ii) Once established, the beatings are stable on a time scale of at least hours.

(iii) Small changes of frequency do not kill the beats, but modify the upper and lower amplitude levels between which the beating occurs; only with a larger change of the driving frequency does the beating disappear

(iv) After changing the frequency, and then bringing it back to its original value, the response is not always completely reproducible: e.g., the beating might reappear only later or, sometimes, not at all.

(v) Beatings were not observed at oscillation amplitudes below the first, or above the second, threshold; but they appeared on both sides of the resonant frequency (see below).

(vi) Beatings were never observed while driving the grid in vacuum.

(vii) Deeper modulation occurred for the case of the virgin grid (see Sec. III D below) than for the cleaned grid.

It seems that beatings can occur at any pressure, but only within a certain defined range of the response amplitude. We did not, however, succeed in establishing any fully repeatable pattern, or well-defined experimental conditions, for the appearance of the phenomenon.

D. Virgin resonant response of the grid in He II

In this subsection we describe the response of the grid to relatively low drives (up to 540 mV_{pp}) when the experiment was performed immediately after pressurizing the cell to the desired pressure at millikelvin temperatures, that is, *without* our having performed the "cleaning" procedure described above.

As seen from Fig. 11, at $p=3.5$ bar, the linewidth measured at the low drive 54 mV_{pp} was about 0.5 Hz as opposed to the ~0.2 Hz for a "cleaned" grid; the observed additional downshift in the resonant frequency would appear to be attributable to this increase in the effective damping of the grid. Otherwise, the response in this range is similar to the regular response obtained from a cleaned grid. However, as indicated for three higher drive levels in Fig. 11, as the response amplitude exceeds about 100 mV_{pp}, the behavior abruptly changes: a sudden onset of beating prevented a smooth continuation of the frequency sweeps in each case. The best and most direct way to visualize this phenomenon was to use the memory oscilloscope. The very robust beating

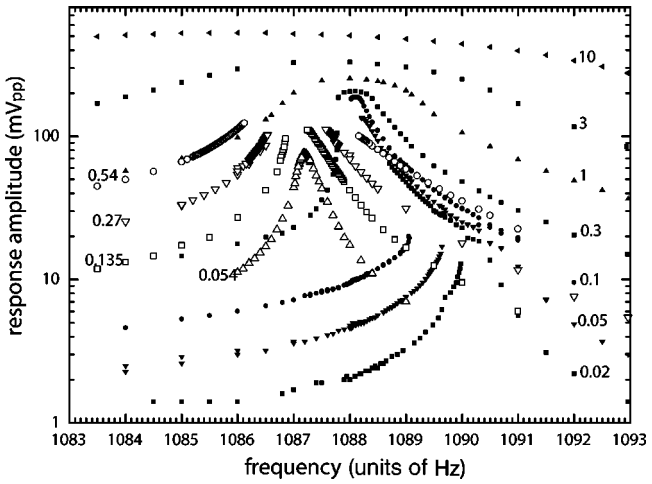

FIG. 11. Resonance curves measured at 3.5 bar using the memory oscilloscope for drive levels (in V_{pp}) as indicated. Filled symbols represent the regular grid behavior obtained with the "cleaned" grid, while the virgin behavior is represented by resonant curves composed of the open symbols. The upper three curves plotted with open symbols are shown up to the drive amplitude at which the onset of beating occurred (see text).

shown in Fig. 10 was obtained under these conditions. The amplitude of the signal grows with time for about 0.45 s roughly proportionally to $\sqrt{t}$, until it reaches the level 126.3 mV_{pp}. At this level the signal amplitude collapses within about 0.2 s to a nearly zero level, and then the whole cycle starts again. We have observed this pattern over a time scale of about an hour, without noticing any appreciable change in its characteristics. For the virgin grid, this structure is reproducible: if one reduces the drive so as to obtain the regular Lorentzian response, and then restores its level back again, the beating pattern reappears.

IV. DISCUSSION

In this section, we aim to discuss the observed phenomena in a physically motivated way in order to identify the key features that an adequate theoretical analysis must be able to encompass. One attempt at such an analysis, via consideration of the dynamics of individual vortex loops, based on the data published in our preliminary report [22], has already been proposed [33], and we summarize its key features in Sec. IV D below. First, however, we discuss possible connections to earlier experiments, discuss the classical behavior seen at low amplitudes, and consider an empirical approach to the intermediate amplitude results based on the concept of an effective boundary layer.

A. Connection to earlier experiments

Reports of earlier experiments of a comparable kind are relatively sparse. A growing shift in resonant frequency with increasing drive was observed in the case of a vibrating sphere in He II by Luzuriaga [12]. Although its origin might be related to the effect observed here, it seems different in character in that there was no definite threshold and the shift did not show a tendency to saturation at high amplitude. The situation was more complicated than here due to two-fluid behavior of He II above 1 K, so it is difficult to identify the connections, if any, between the observed phenomena.

Morishita and coauthors [21] carried out an interesting experimental study of a thin vibrating wire in He II under conditions comparable to ours. Although they were mainly concerned with mean free path effects at higher temperatures, the authors reported hysteresis below 70 mK that became larger with increasing drive level. No satisfactory explanation could be offered. The observed hysteresis was qualitatively different from that reported here, in that it set in gradually rather than abruptly on reaching a threshold; nor did the frequency shift cease at a second threshold. In addition, given that their experiment involved a NbTi wire oscillating in a magnetic field of order of its first critical field H_{c1}, it was impossible to exclude the possibility that some of the observed hysteresis might have been connected with the superconducting nature of the wire itself. Rather similar effects, most likely attributable to the nucleation of quantized vortex lines both in He II [34] and in superfluid ^{3}He–B [35–37], have been observed over the years in experiments with vibrating wires.

We emphasize that the present study refers to *macroscopic* flow and turbulence of the superfluid. Where influenced by vorticity, the results reported represent an average over a large ensemble of quantized vortices. It should therefore be reproducible, and independent of the positions/configurations of individual vortex lines. We consider first the behavior seen at relatively low velocities, which we assume to be unaffected (or almost unaffected: see below) by the presence of vortices.

B. Frequency shift at small amplitudes

The data of Figs. 4, 5, and 7 show that, for small drive amplitudes, the resonant frequency is almost amplitude independent, but shifted down by $\sim$30 Hz from its vacuum value. We can account for this effect in terms of the classical hydrodynamic effective mass.

We start by approximating the actual motion of the grid as one dimensional, as in our preliminary report [22]. Although simplified [38], this approach may nonetheless be expected to provide useful insight into underlying physical processes involved in the superflow under study. The one-dimensional equation of motion for the grid oscillating in a vacuum then takes the simple form of a driven linear oscillator

$$M\ddot{z} + D\dot{z} + Kz = F_0 \cos(\omega t) \tag{3}$$

responding at the driving frequency $\omega = 2\pi f$. In vacuum the damping coefficient D reflects the nuisance damping only and M denotes the bare mass of the grid; the restoring term Kz comes from the tension in the grid [27]. On sweeping the drive frequency slowly through the resonant frequency, given in the limit of low damping by $f_0 \cong 1/2\pi\sqrt{K/M}$, we expect to obtain a Lorentzian curve of narrow linewidth.

Driving the grid in an ideal fluid (corresponding to pure superfluid He II with no remanent vorticity), the effective mass of the grid becomes hydrodynamically enhanced [39]

by $\Delta M = \beta V \varrho_{\mathrm{He}}(p)$, which will result in a downshift of the resonant frequency by Δf, from f_0 to $f_1(p)$. Here V is the volume of the grid and the dimensionless factor β can be evaluated as

$$\beta \cong \varrho_{\mathrm{Ni}}/\varrho_{\mathrm{He}}(p)[f_0^2/f_1(p)^2 - 1]. \tag{4}$$

Experimentally, $\Delta f \ll f_0$, so, expanding and retaining only the linear term, we expect a linear dependence of Δf on $\varrho_{\mathrm{He}}(p)$, which is tabulated in Ref. [40]. As shown in Fig. 8, this is indeed the case: fitting this dependence leads to a value of $\beta = (3.01 \pm 0.05)$. Taking into account the complex geometry of the grid (see Fig. 2), it seems not inconsistent with the facts that $\beta = 0.5$ for a sphere and $\beta = 1$ for an infinitely long cylinder. We do not know of calculations for a body of rectangular cross section—let alone for the actual cross section of the grid—but, if we approximate a grid wire by an infinite elliptic cylinder of axes a and b moving in the direction along its short axis b, and if $a/b = 3$, then $\beta = 3$ [39]. The superimposed vacuum resonances in Fig. 4, like those in Fig. 2 of Ref. [22], show that no appreciable increase in damping occurs in the limit of low drive: the He II just serves as a mechanical vacuum [41] whose only physical effect is a renormalization of the mass. The excess damping due to any remanent vortex lines that may still be present [42], even in the case of the cleaned grid, is evidently beyond our resolution. We shall return to a question of a possible frequency shift due to these remanent vortex lines later.

Nonetheless, remanent vorticity provides the most likely explanation of why the "cleaned" and "virgin" behaviors of the grid are so different. Increasing the pressure in the cell presumably leads to the generation/injection of quantized vortices by the jet of superfluid entering the cell from the filling capillary. They are likely to reconnect with each other and with image vortices in walls and electrodes, leaving remanent vorticity pinned to the grid or between the grid and the surrounding electrodes. It is probably these vortices that cause the additional downshift of resonant frequency in the low drive limit and the appreciable broadening of the resonance peak (see Fig. 11). We shall return to the "virgin" grid behavior below. First we concentrate on the regular flow due to a "cleaned" grid.

C. Amplitude-dependent frequency shift above the first threshold: Macroscopic approach

With increasing response amplitude, the regular behavior of the driven grid acquires highly nonlinear features, as we have seen, and between the first and second thresholds the resonant frequency shifts further down by about 2 Hz, independently of the applied pressure (Figs. 8 and 9). Within our simple model with negligibly low damping, the resonant frequency $\sim\sqrt{K/M}$ can be shifted down *either* by a decrease of the spring constant K of the grid, *or* by a further enhancement of the hydrodynamic effective mass [43] $M_{\mathrm{eff}} = M + \Delta M(p)$. There is no obvious mechanism by which the presence of the liquid could change the effective spring constant. We are therefore left with the conclusion that the additional downshift of about 2 Hz observed above the first threshold arises from a *further* enhancement of the effective mass of the grid, i.e., an enhancement additional to the classical hydrodynamic enhancement [39] discussed in the preceding subsection.

Given the essential simplicity of the superfluid in the $T \to 0$ limit, and the scarcity of excitations, we seem forced to conclude that the increased effective mass is in some way associated with quantized vortices. We speculate that, on exceeding the first threshold, a "boundary layer" of vortex loops builds up on the grid, somehow increasing its inertia. This would cause the resonant frequency to shift down with increasing amplitude and the resonance curves to acquire the strongly nonlinear features that are observed. Let us suppose that, as occurs in classical viscous fluids, a boundary layer of thickness λ is formed, enhancing the hydrodynamic effective mass of the grid by $\Delta M_g^{\lambda} = A\lambda\varrho_{\mathrm{He}}(p)$, where A denotes the surface area of the grid. Requiring that the downward shift of the resonance frequency corresponds to those observed experimentally we have

$$\lambda(p) = \frac{M + \Delta M_g^{\lambda}}{A\varrho_{\mathrm{He}}(p)}\left(\frac{f_1^2}{f_2^2} - 1\right). \tag{5}$$

The values of $\lambda(p)$ required to account for the maximum frequency downshift are given in Table II. A statistical analysis leads to $\lambda = (0.53 \pm 0.05)\ \mu$m, although there seems to be a slight tendency for $\lambda(p)$ to decrease with increasing pressure. Note that the boundary layer thickness is much smaller than any linear dimension of the grid windows. At first sight, therefore, it might be reasonable to approximate the behavior in terms of a classical-like boundary layer covering the moving surface.

From the calculated thickness of the effective boundary layer, we can formally calculate an effective kinematic viscosity, requiring $\lambda(p) = \sqrt{2\nu_{\mathrm{eff}}(p)/\omega}$ and the dynamic viscosity $\eta_{\mathrm{eff}}(p) = \varrho(p)\nu_{\mathrm{eff}}(p)$. These quantities are plotted versus pressure in Fig. 12. These are the viscosities that would be needed to produce a change in effective mass sufficient to cause the observed frequency shift if the grid were oscillating in a hypothetical viscous fluid, not in a superfuid. Note in passing that the calculated value of this effective kinematic viscosity is three orders of magnitude below that of water, and a factor of 20 below that of normal liquid He I just above the lambda transition [46]. Extending the analogy, we may also estimate the expected linewidth of the resonance peak due to the drag of such a hypothetical viscous fluid. A straightforward calculation [47], approximating the flow velocity gradient in the fluid by $\langle v_g \rangle/\lambda$, leads to a linewidth ~ 1 Hz. The strongly nonlinear curves corresponding to drive levels slightly exceeding the first threshold *do not*, however, display any appreciable increase in damping, in the sense that the response at maximum remains proportional to the drive (see Fig. 6). This suggests that, until the response amplitude reaches the second threshold, none of the vortex loops that we suppose to comprise the boundary layer can carry away any energy by leaving the grid. These ideas are developed in more detail in Sec. IV D below, describing a recently proposed theory [33] that effectively replaces the concept of an effective kinematic viscosity.

TABLE II. Calculated values characterizing the macroscopic properties of the He II flow due to oscillating grid (assuming its motion is one dimensional) at various pressures at low temperature: v_1 and v_2 are the estimated peak flow velocities corresponding to the first and second critical thresholds; ϱ_{He} denotes the density [40] of He II; β is the hydrodynamic enhancement factor (see text); λ denotes the required thickness of the boundary layer; and ν_{eff} is the calculated value of the effective kinematic viscosity.

p (bar)	v_1 (cm/s)	v_2 (cm/s)	ϱ_{He} (g/cm^3)	β	λ (μm)	ν_{eff} (cm^2/s$\times 10^5$)
0.30	0.302	2.87	0.1456	2.95	0.63	1.35
2.20	0.292	2.87	0.1488	2.97	0.56	1.07
3.50	0.295	2.85	0.1508	2.94	0.62	1.31
5.05	0.260	2.86	0.1529	2.95	0.55	1.04
5.50	0.302	2.89	0.1535	2.96	0.53	0.95
10.00	0.295	2.89	0.1589	3.07	0.52	0.93
10.09	0.265	2.87	0.1590	3.07	0.50	0.86
12.05	0.245	2.90	0.1611	3.06	0.49	0.83
14.00	0.242	2.90	0.1631	3.03	0.53	0.95
15.50	0.365	2.86	0.1646	3.07	0.43	0.64
15.55	0.158	2.89	0.1646	3.06	0.47	0.75
18.00	0.135	2.92	0.1668	3.02	0.55	1.03
19.95	0.152	2.86	0.1685	3.03	0.54	0.99
24.79	0.148	2.93	0.1723	3.04	0.52	0.91

It is interesting to characterize the first threshold in terms of a superfluid Reynolds number $\mathrm{Re}_s = R_{\mathrm{ch}} U_{\mathrm{ch}} / \kappa$, where R_{ch} and U_{ch} stand, respectively, for a length scale and velocity characteristic of the superflow in question, and $\kappa = 0.000\,997$ cm^2/s denotes the quantum of circulation. To estimate the critical value of Re_s^I associated with the first threshold, we believe it is natural to use the peak flow velocity averaged over a grid window in the frame of reference of the grid. The observed values of the first critical amplitude are given in Table I for all investigated pressures. We have converted the peak value of the *grid velocity* to the peak *flow velocity* by multiplying by a numerical factor ≈1.43 to allow for the 70% grid transparency, assuming that the grid motion is one dimensional (see column v_1 in Table II). If one also takes into account that the vertical displacement profile of the grid, when vibrating in its fundamental axisymmetric mode, is given in the radial direction by the zeroth order Bessel function $J_0(2.4048r/R)$, the peak flow velocity (i.e., U_{ch}^I) through its center is further enhanced by a factor ≈2.3. As a characteristic length scale R_{ch}^I we use the size of the individual bars composing the grid. The superfluid Reynolds number associated with the first threshold, $\mathrm{Re}_s^I = R_{\mathrm{ch}}^I U_{\mathrm{ch}}^I / \kappa$, is displayed in Fig. 13. Note that, although it decreases with increasing pressure, it is of order unity for all pressures, in qualitative agreement with the famous Feynman criterion

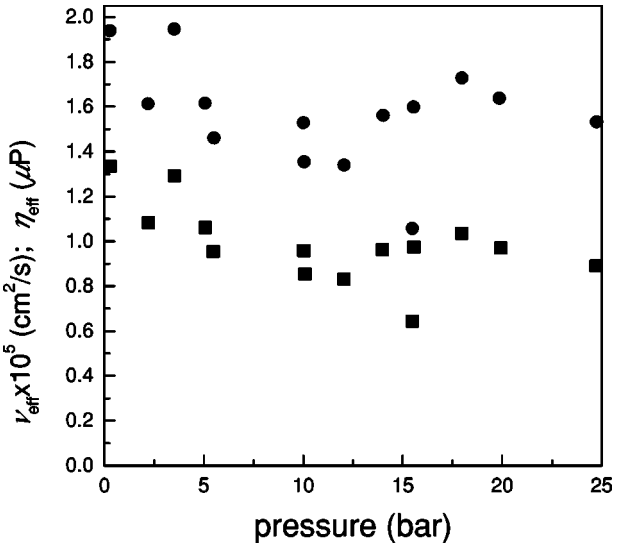

FIG. 12. Calculated values of the effective kinematic viscosity (squares) and dynamic viscosity (circles) versus pressure.

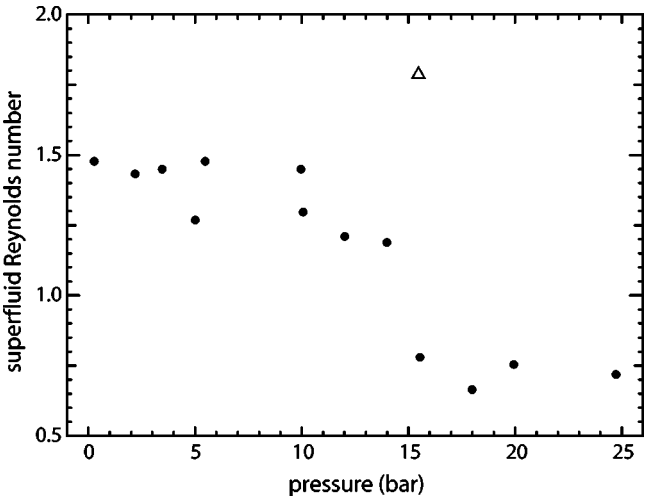

FIG. 13. The superfluid Reynolds number Re_s^I corresponding to the first critical threshold, plotted versus the pressure. The "anomalous" triangular data point is discussed in the text.

based on the value of self-induced velocity for a vortex loop of the size of the grid bar.

The experimental point plotted for $p=15.5$ bar (the open triangle) falls in a seemingly anomalous position. We are aware of only one experimental difference from the conditions under which the other data were recorded: the drive dependence of the resonant response had just previously been measured up to the highest available drive amplitudes. This involved use of the transformer to boost the driving potential (by a factor of $\simeq 27$). This unusually high drive probably resulted in more efficient "cleaning" than the standard procedure of shaking the grid with the 10 V_{pp} directly available from the signal generator. This observation supports the idea that driving the grid at high amplitude causes a re-arrangement of remanent vorticity rather than its total removal.

D. Amplitude-dependent frequency shift above the first threshold: Microscopic approach

The macroscopic approach above, based on analogy with the boundary layer theory for classical fluids, fails to explain why the damping above the first threshold remains apparently unchanged. The main challenge for any microscopic theory based on vortex dynamics is (i) to explain the mechanism that gives rise to the amplitude-dependent effective mass, and (ii) to show how this effect can occur without any corresponding increase in damping. A possible approach to these problems has been proposed in Ref. [33], and we now summarize briefly the main ideas.

The character of the dynamical response of a vortex loop attached to a grid oscillating at the drive frequency ω will depend on whether it is significantly longer or shorter than the minimum resonant length $\ell \approx 13$ μm required by the well-known dispersion relation

$$\omega(k) = \omega\left(\frac{2\pi}{\ell}\right) \cong \frac{\kappa k^2}{4\pi} \ln\left(\frac{1}{ka_0}\right) \tag{6}$$

for a Kelvin wave [2], where a_0 is the vortex core parameter. If the loop is shorter than ℓ, it will respond adiabatically, in that its position and configuration in the flow will always correspond to equilibrium. For loops that are significantly longer than ℓ, on the other hand, Kelvin waves will be excited, leading to dissipation. Dissipation may thus occur either through the transfer of energy via a Kelvin wave cascade [17] to very high frequencies, at which there can be significant phonon radiation, or through the loss of vortex rings as the result of reconnections. It appears likely, therefore, that these longer vortex loops (probably including some connecting the grid to the neighboring electrodes) are being removed during the "cleaning" procedure described above.

It can be shown [33] that, when a vortex loop is pinned by both ends to the grid and responds adiabatically, it enhances the effective mass of the grid by $\varrho_{\mathrm{He\ II}}\kappa(dS/dv)$, without increasing the damping. Here $S(v)$ is the area between the loop and the neighboring walls. For small velocities, $S(v)$ is probably a linear function of the flow velocity v, and the overall effect is a constant, amplitude-independent, enhancement of the effective mass of the grid. If $S(v)$ were to become nonlinear at the first threshold, however, the observed highly nonlinear form of the measured resonance curves can be accounted for: it would be necessary for the nonlinear part of the loop area to contribute ~ 2500 μm^2 per window of the grid at the second threshold [33]. It follows that mass enhancement through this mechanism cannot be due to a single loop—it would simply be too long to respond adiabatically. In fact, if one considers also the stability of these loops against "ballooning out" below the second threshold, the analysis [33] suggests a dense boundary layer constituted of small loops, with $\sim 10^3$ per grid aperture, i.e., about 10^8 loops altogether, each sized ~ 1 μm or less.

Note in passing that, at higher temperature where there is an appreciable fraction of normal fluid, such a flow involving a boundary layer of small vortex loops would be dissipative, and not only because the grid is moving through a normal fluid of finite viscosity. On length scales comparable with the distance between the vortex loops constituting the boundary layer, the normal and superfluid velocity fields cannot be fully matched and the resulting mutual friction will assure dissipation of the flow energy. The interesting question of just how such a process sets in remains open as a subject for future investigation.

It is tempting to suppose that the formation of this boundary layer is intrinsic to any superflow over a solid boundary. Perhaps, employing the ideas of Kusmartsev [44], the boundary layer can grow from a "plasma" of half vortex rings, although the critical velocities derived by Kusmartsev are much larger than those considered here. The difficulties associated with intrinsic vortex nucleation are well established [45] and intrinsic critical velocities in microscopically small channels are assumed to be ~ 30 m/s at low temperature. Here, on the other hand, we have an open geometry, the grid surface is very rough and substantial enhancement of flow around excrescences is possible. The nucleation problem, discussed above in relation to the drive dependence of the response amplitude at resonance, is consistent with this picture.

Another possibility is to suppose that the boundary layer is essentially extrinsic, in that the generation of quantized vortex loops on the surface of the grid by macroscopic superflow around it probably involves growth from remanent vortex lines [42] and may well be produced by the "cleaning" procedure that causes the "virgin" and "regular" behaviors to differ.

At present, the available experimental data do not allow us to resolve this interesting and fundamental issue. There is a clear call for more precise studies of the "cleaning" procedure, possibly involving grids with different geometry and surface roughness.

E. Onset of dissipation

As we have seen, a dissipative process sets in at a response level corresponding to the second critical threshold: on increasing the drive further, the main result is an increase in linewidth (see Figs. 4 and 5). Under these flow conditions, the He II is behaving in close analogy with a classical Navier-Stokes fluid, in that the flow is dissipative. Using the

observed values of the response amplitude for the second threshold from Table I we can conclude that it does not depend appreciably on pressure, and reaches 190 ± 2 mV_{pp}.

Let us now discuss the second, pressure-independent threshold in terms of a superfluid Reynolds number $Re_s^{II}=R_{ch}^{II}U_{ch}^{II}/\kappa$. In the classical case, steady flow through a grid generates turbulence that is nearly homogeneous and isotropic—the turbulent wakes created at grid bars coalesce at some distance downstream. One usually characterizes such a flow by a mesh Reynolds number, i.e., the mesh size of the grid plays the role of the characteristic distance. Below the second threshold, however, we are dealing with an oscillating (super)flow of relatively small amplitude (up to the size of a grid bar). Flow around the bar on one side of a grid aperture will therefore be almost unaffected by flow around the bar on the other side of the aperture. Use of the mesh size as a characteristic length scale therefore seems inappropriate. We suggest that the relevant superfluid Reynolds number characterizing the onset of superfluid turbulence at the second threshold be defined in the same way as was done above for the first threshold. Calculation of the peak velocity for the second threshold by the above procedure results in $U_{ch}^{II}=6.6\pm0.1$ cm/s and assuming $R_{ch}^{II}=R_{ch}^{I}$ we arrive at $Re_s^{II}\approx14$.

The observed values of Re_s^{II} compare well with the critical $Re_s=UD/\kappa\approx20$ (U is the transport velocity and D the diameter of the pipe) found as a temperature-independent threshold in pipe flow of He II at much higher temperatures when the flow of the normal component was inhibited by superleaks placed at both ends of the pipe [48]. This suggests that, although the underlying physical mechanism leading to a transition to superfluid turbulence is not well understood, it probably remains unchanged even at temperatures above 1.4 K where there is an appreciable fraction of normal fluid.

Microscopic considerations based on the dynamic response of individual vortex loops relevant to the onset of dissipation can be found in [33]. To resolve this complicated issue fully, however, further more work is needed, including computer simulations on dynamic behavior of pinned vortex loops subject to an oscillatory superflow.

The square-root behavior (see the inset in Fig. 6) of the resonant response as a function of drive amplitude above the second threshold is typical of classical turbulent drag scaling. It is therefore most likely that this threshold marks the onset of turbulence. The dissipation process might be analogous to the evaporation of a packet of quantized vorticity [49] proposed to explain turbulent behavior [50] of superfluid ^{3}He-*B*.

F. Amplitude modulation "beating" phenomena

Let us consider possible origins of the beating phenomena (see Fig. 10, and Fig. 2 of Ref. [22]) with properties summarized above. We recall that, in the "regular" regime, they are observed at the response amplitude between the first and second thresholds on both sides of the resonant frequency. The most pronounced beatings are observed (Fig. 10) above a critical amplitude (Fig. 11) when probing the virgin behavior of the grid. Given the similar appearance and time scales of beatings within the regular and cleaned regimes, we will assume for now that they have a common origin. As already mentioned above, we associate the difference between the virgin/regular behaviors with the presence/absence of remanent quantized vortices in significant numbers. The linewidth at low drive (virgin behavior) is broader than that observed either in vacuum or in He II (regular behavior), and the resonant frequency is shifted down relative to the latter. We infer that the observed phenomena are a direct consequence of quantum vortices adjacent to the grid, pinned in some random fashion.

We may therefore attempt to explain the observed beatings on the assumption that, on reaching the critical response amplitude (126.3 mV_{pp} in the particular case described above) the oscillatory motion of the grid almost stops within a period of ~0.2 s by generation of a vortex tangle. It means that the energy of the moving grid with peak velocity given by its critical response amplitude, of order 0.01 μJ, is transformed to vortex line of total length ~5 km. Assuming further that the tangle spreads and decays away at a sufficiently high rate, it corresponds to a steady heat input to the cell of $\simeq0.01-0.1$ μW. Notwithstanding the linkage of the He II sample (via a complicated set of thermal links including the Kapitza resistance) to the mixing chamber of the dilution refrigerator, this would have led to appreciable warming of the sample (30 to 50 mK in about 15 min, just considering heat capacity).

In practice, no appreciable increase of the cell temperature was observed on the time scale of one hour while observing the stable beating pattern. If the motion of the grid is approximated as one dimensional [22], then we are obliged to interpret the behavior of Fig. 10 in this way, but it is an approach that evidently fails to provide a plausible explanation for the beating phenomenon.

We point out that it may, however, be necessary to consider the dynamics of our oscillating grid in more detail. It represents a nearly homogeneous oscillating membrane under uniform tension. The electrostatic driving force resulting from applying the ac voltage to the upper electrode can be assumed as nearly uniformly distributed over the entire grid area. Thus, as already pointed out in Sec. IV C driving the grid at a frequency near its fundamental resonance should result in a particularly simple axially symmetric oscillation pattern, with a vertical displacement profile in the radial direction given by the Bessel function $J_0(k_r r)$, with the wave vector k_r chosen in such a way that the displacement vanishes at the circumference of the grid, $r=R$. This spatial displacement profile ought to be relevant when driving the grid in vacuum and in He II for amplitudes below the first threshold, i.e., up to response signal amplitudes not exceeding ~10 mV_{pp}. As the oscillation amplitude increases, the threshold will first be reached initially in the middle of the grid [51], where quantum vortex loops will cause a local enhancement of the effective mass per unit area. Consequently, the spatial displacement profile will depart from that given by the Bessel function $J_0(k_r r)$.

Assuming that the axial symmetry is maintained, the resonant frequency of the stationary response curve ought gradually to shift down, in accord with the experiment. If the vortex loops composing the boundary layer do not leave the grid

carrying its energy away, there is no reason to expect any broadening of the peak at this stage: its width should remain at the nuisance damping (i.e., vacuum) level.

In reality the vortex loops will probably locally enhance the effective mass of the grid in a way that breaks the axial symmetry. The grid can therefore no longer be well approximated as an oscillating membrane of homogeneous areal density, but represents a rather complex nonlinear oscillatory system. A simple stationary response to a spatially uniform drive might no longer exist and, conceivably, this could show up experimentally as beatings between two different amplitude values. We may expect that, for any given configuration of vortex loops, the beating pattern would be reasonably stable in that small changes in the drive would only change the average sizes of existing loops, but not their overall geometrical configuration. Consistent with this idea, there is a high degree of reproducibility of the response for a given frequency and drive when the range of the frequency sweeps is sufficiently small. Faster and bigger changes in frequency probably lead to a more drastic spatial rearrangement of the vortices that constitute the boundary layer. On bringing the frequency back to its original value, following an excursion of this kind, a different spatial configuration might be produced, leading either to a different beating pattern or to the disappearance of beating. This qualitative discussion of the beatings described in Sec. III C is consistent with the observations that beatings are never observed in vacuum, and only occur above the first threshold in He II.

On increasing the amplitude further, the second threshold will eventually be reached in the central area of the grid. Note that the second threshold is ten times higher than the first one so, by this time, most of the grid area will be oscillating with an amplitude exceeding that of the first threshold. Thus its mass per unit area is already enhanced by the existence of the effective boundary layer. It would seem that, when the second threshold is attained by the central part of the grid, an additional damping force will start to act locally, in the central area of the grid; presumably it suffers a phase shift [47] (which for a viscous fluid would be $\pi/4$). Further increase in the the oscillation amplitude is no longer proportional to the drive but almost ceases due to the very rapid increase in damping. Only for much higher drives, when the damping area becomes almost the size of the entire grid, does a new regular pattern become established. This time, the turbulent-like drag is characterized by a square-root dependence of the response on the drive amplitude.

These considerations allow us to speculate about a possible alternative scenario that might account for the beatings (Fig. 10). Additional damping in the central area of the grid will tend to flatten the displacement profile. The resultant force in the central area of the grid will become more and more phase shifted. It is possible to envisage that, with a further increase in drive, this phase shift may grow until a transition occurs into a vibration regime where the middle of the grid and its outer annulus oscillate in opposite directions, mutually in antiphase, i.e., similarly as in the (0,2) oscillatory mode. Due to energy conservation the oscillating amplitude (or, rather, its mean-square value averaged over the entire grid area) ought to stay roughly constant. However, our detection method consists of measuring the induced voltage on a lower electrode that covers the entire grid area. For the same response amplitude, therefore, the signal induced in the (0,1) mode will be vastly greater than that in an (0,2)-like mode. So what appears (Fig. 10) as a drastic reduction in the oscillatory amplitude may in reality correspond to a continuous transition to a (0,2)-like mode. At present we cannot decide which scenario is more likely; further experimental work, backed up by simulations and theoretical investigations, is required to resolve the issue.

V. SUMMARY

We have reported a systematic experimental investigation of the macroscopic flow of pure He II in the limit of very low temperature, using a vibrating grid as a probe. Our results confirm that for flow velocities below a threshold value, He II can indeed behave as an ideal fluid: its presence enhances the hydrodynamic mass of the oscillating body, without making a measurable contribution to the damping. After the injection of extra liquid through an increase of pressure at low temperature, however, the He II *does* contribute additional damping, observed as a downshift in resonance frequency and an increase of the linewidth, even in a limit of low driving force. We attribute this effect to an increased level of remanent vorticity engendered by the jet of He II issuing from the filling capillary as the cell is being pressurized. The effect can be substantially reduced by violently shaking the grid—presumably causing remanent vorticity to be shaken off or rearranged in some way—following which procedure the resonance frequency is found to have shifted up, with a corresponding decrease of linewidth indistinguishable from its vacuum value. The response then remains stable on a time scale of at least days.

On increasing the flow velocity above the first threshold (characterized by a flow velocity of a few mm/s or by a superfluid Reynolds number of order unity) an effective boundary layer comprised of quantized vortices enhances the hydrodynamic effective mass of the grid but not the damping which, in the zero temperature limit, remains unchanged until the second threshold (characterized by a flow velocity of a few cm/s or by the superfluid Reynolds number $\sim 10-20$) is attained, which is where dissipation sets in. Intriguing effects such as pronounced beatings have been observed in this range of response amplitudes and, currently, these are only partly understood.

Further increase of the drive leads to a viscouslike dissipative flow. It can perhaps be understood as He II mimicking the boundary layer that arises in oscillatory viscous flow in a classical fluid: in the case of He II this would involve an appropriate rearrangement of vortex loops in the vicinity of the solid boundary, analogous to the way in which a rotating bucket of He II at sufficient angular velocity imitates solid body rotation. For the highest achievable drives, the flow can be characterized as developed superfluid turbulence. The velocity grows in proportion to the square root of the drive, i.e., the quantized vorticity being generated leads to a turbulent drag dependence typical of classical viscous fluids.

We are aware that there are a number of problems and unanswered questions, such as the universality of the ob-

served phenomena, the intrinsic versus extrinsic origin of the effective boundary layer, the pressure dependence of the first threshold, and a more detailed characterization of the influence on flow of the remanent vorticity. There is also a clear call to investigate how the observed phenomena change with increasing temperature, and relevant experiments have already been started.

We hope that these results will stimulate further effort, both experimental and theoretical, leading to a better understanding of the underlying physics of superflow and of the nucleation of quantum and possibly even classical turbulence.

ACKNOWLEDGMENTS

We are very grateful to N. J. Fullwood for making the electron micrographs of the grid, and to A. M. Guénault for setting up automatic data logging for us using the lock-in amplifier. It is a pleasure to acknowledge fruitful discussions with many colleagues, especially including D. I. Bradley, D. Charalambous, A. M. Guénault, R. P. Haley, M. Krusius, G. R. Pickett, P. Skyba, and W. F. Vinen. The research was supported by the Engineering and Physical Sciences Research Council (U.K.) and by the Czech Grant Agency under Grant No. GAČR 202/02/0251.

[1] J. T. Tough, Prog. Low Temp. Phys. **8**, 133 (1982).
[2] R. J. Donnelly, *Quantized Vortices in Helium II* (Cambridge University Press, Cambridge, U.K., 1991).
[3] *Quantized Vortex Dynamics and Superfluid Turbulence*, edited by C. F. Barenghi, R. J. Donnelly, and W. Vinen (Springer, Berlin, 2001).
[4] L. Landau, J. Phys. (USSR) **5**, 71 (1941).
[5] L. Landau, J. Phys. (USSR) **11**, 91 (1947).
[6] T. Ellis and P. V. E. McClintock, Philos. Trans. R. Soc. London, Ser. A **315**, 259 (1985).
[7] P. C. Hendry, N. S. Lawson, P. V. E. McClintock, C. D. H. Williams, and R. M. Bowley, Phys. Rev. Lett. **60**, 604 (1988).
[8] E. Varoquaux, O. Avenel, Y. Mukharsky, and P. Hakonen, in *Quantized Vortex Dynamics and Superfluid Turbulence*, edited by C. F. Barenghi, R. J. Donnelly, and W. F. Vinen (Springer-Verlag, Berlin, 2001), pp. 36–50.
[9] D. V. Osborne, Proc. Phys. Soc. London **63**, 909 (1950).
[10] J. Jäger, B. Schuderer, and W. Schoepe, Phys. Rev. Lett. **74**, 566 (1995).
[11] M. Niemetz, H. Kerscher, and W. Schoepe, J. Low Temp. Phys. **126**, 287 (2002).
[12] J. Luzuriaga, J. Low Temp. Phys. **108**, 267 (1997).
[13] M. R. Smith, D. K. Hilton, and S. V. Van Sciver, Phys. Fluids **11**, 751 (1999).
[14] J. Maurer and P. Tabeling, Europhys. Lett. **43**, 29 (1998).
[15] M. R. Smith, R. J. Donnelly, N. Goldenfeld, and W. F. Vinen, Phys. Rev. Lett. **71**, 2583 (1993).
[16] S. R. Stalp, L. Skrbek, and R. J. Donnelly, Phys. Rev. Lett. **82**, 4831 (1999).
[17] W. F. Vinen, Phys. Rev. B **61**, 1410 (2000).
[18] W. F. Vinen and J. J. Niemela, J. Low Temp. Phys. **128**, 167 (2002).
[19] L. Skrbek, J. J. Niemela, and R. J. Donnelly, Phys. Rev. Lett. **85**, 2973 (2000).
[20] L. Skrbek, A. V. Gordeev, and F. Soukup, Phys. Rev. E **67**, 047302 (2003).
[21] M. Morishita, T. Kuroda, A. Sawada, and T. Satoh, J. Low Temp. Phys. **76**, 387 (1989).
[22] H. A. Nichol, L. Skrbek, P. C. Hendry, and P. V. E. McClintock, Phys. Rev. Lett. **92**, 244501 (2004).
[23] P. C. Hendry and P. V. E. McClintock, Cryogenics **27**, 131 (1987).
[24] The extreme isotopic purity was necessary [25] in view of an associated experiment using negative ions to probe the tangle of quantized vorticity believed to be created by large-amplitude oscillations of the grid. It is not known what level of isotopic purity was necessary for the present experiment; but, in earlier studies [26] of vortex creation by negative ions, ^{3}He at isotopic ratios of $\sim 10^{-9}$ exerted a measurable effect on the creation rate.
[25] R. M. Bowley, G. G. Nancolas, and P. V. E. McClintock, Phys. Rev. Lett. **52**, 659 (1984).
[26] G. G. Nancolas, R. M. Bowley, and P. V. E. McClintock, Philos. Trans. R. Soc. London, Ser. A **313**, 537 (1985).
[27] M. I. Morrell, M. Sahraoui-Tahar, and P. V. E. McClintock, J. Phys. E **13**, 350 (1980).
[28] We have checked the reduction factor by adding extra lengths of coaxial cable of known capacitance.
[29] This statement is valid for the fundamental mode of vibration; clearly, it does not hold if higher modes become excited.
[30] While driving the grid hard in He II, additional oscillation modes can be excited and observed. At modest drive levels, however, their resonant amplitude is more than two orders of magnitude lower than that of the fundamental and they appear as small but clearly observable glitches on both sides of the resonance peak.
[31] In our preliminary report [22] we have overestimated the grid velocity by a factor of 4, due to an error in derivation of Eq. (2).
[32] We cannot exclude that while driving the grid in vacuum at a high amplitude its temperature rises, as the thermal link to the cell is extremely weak. This can cause changes in elastic behavior of the oscillating grid.
[33] W. F. Vinen, L. Skrbek, and H. A. Nichol, J. Low Temp. Phys. **135**, 423 (2004).
[34] A. M. Guénault (private communication).
[35] D. I. Bradley, Phys. Rev. Lett. **84**, 1252 (2000).
[36] M. Niemetz, W. Schoepe, and M. Krusius, Phys. Rev. Lett. **87**, 059601 (2001).
[37] D. I. Bradley and G. R. Pickett, Phys. Rev. Lett. **87**, 059602 (2001).
[38] By neglecting the radial displacement profile in approximating the grid motion as one dimensional, one underestimates the peak velocity at its geometrical center by a factor $\simeq 2.3$, as discussed later.
[39] H. Lamb, *Hydrodynamics* (Cambridge University Press, Cam-

bridge, U.K., 1932).
[40] J. S. Brooks and R. J. Donnelly, J. Phys. Chem. Ref. Data **6**, 51 (1977).
[41] T. Ellis and P. V. E. McClintock, Phys. Lett. **89A**, 414 (1982).
[42] D. D. Awschalom and K. W. Schwarz, Phys. Rev. Lett. **52**, 49 (1984).
[43] Note that a similar effect could be accounted for through an increase in the damping constant, assuming it to be imaginary. The resulting shift would have a different frequency dependence, linear in ω rather than quadratic. Unfortunately, within the narrow accessible range of ω, we cannot distinguish between the two dependences.
[44] F. V. Kusmartsev, Phys. Rev. Lett. **76**, 1880 (1996).
[45] E. Varoquaux and O. Avenel, Phys. Rev. B **68**, 054515 (2003).
[46] R. J. Donnelly and C. F. Barenghi, J. Phys. Chem. Ref. Data **27**, 1217 (1998).
[47] L. D. Landau and E. M. Lifshitz, *Fluid Mechanics* (Butterworth and Heinemann, Oxford, 1987).
[48] M. L. Baehr, L. B. Opatowsky, and J. T. Tough, Phys. Rev. Lett. **51**, 2295 (1983).
[49] C. F. Barenghi and D. C. Samuels, Phys. Rev. Lett. **89**, 155302 (2002).
[50] S. N. Fisher, A. J. Hale, A. M. Guénault, and G. R. Pickett, Phys. Rev. Lett. **86**, 244 (2001).
[51] Given the rough surface of the grid, the nucleation centers are probably more or less randomly distributed over its whole area. Simple analysis then shows that the highest probability of reaching a threshold is along a circle of $r \approx 0.4R$ and thus close to the node circle if the grid were to oscillate in the axisymmetric (0,2) mode.